Journal of the European Ceramic Society **13** (1994) 103–111

Low Temperature Superplastic Flow of Yttria Stabilized Tetragonal Zirconia Polycrystals

M. M. R. Boutz, A. J. A. Winnubst,* A. J. Burggraaf

University of Twente, Faculty of Chemical Technology, Laboratory for Inorganic Chemistry, Materials Science and Catalysis, P.O. Box 217, 7500 AE Enschede, The Netherlands

&

M. Nauer,‡ C. Carry§

Laboratoire de Céramique, Ecole Polytechnique Fédérale de Lausanne, CH 1015 Lausanne, Switzerland

(Received 22 July 1993, revised version received 22 October 1993, accepted 12 November 1993)

Abstract

Very fine grained (0.2 μm), dense Y-TZP ceramics have been produced by free sintering at 1150 °C. The superplastic deformation of these materials is studied in compression at low temperatures (1100–1300 °C). A significant enhancement in initial strain rates was observed compared to a coarser-grained (0.4 μm) commercially available material (Tosoh, Japan). Doping with small amounts of Fe_2O_3 led to a further enhancement of strain rate. Deformation occurred via interface reaction controlled grain boundary sliding. Prior to deformation a continuous glassy silicate film was observed at the grain boundaries. The applicability of interface reaction controlled solution–precipitation creep models is discussed. The absence of a steady state during deformation at low stresses is attributed to dewetting of the silicate film.

Sehr feinkörnige (0.2 μm), dichte Y-TZP Keramiken wurden bei 1150 °C gesintert. Die superplastische Verformung dieser Materialien wurde bei niedrigen Temperaturen (1100–1300 °C) in Kompression untersucht. Es zeigte sich eine deutliche Erhöhung der Anfangsdehnraten im Vergleich zu grobkörnigem (0.4 μm), kommerziell erhältlichem Material (Tosoh, Japan). Die Dotierung mit geringen Mengen Fe_2O_3 ergab eine weitere Steigerung der Dehnrate. Die Verformung erfolgte mittels Korngrenzengleitung kontrolliert durch die Grenzflächenreaktion. Von der Verformung konnte ein kontinuierlicher, glasartiger Silikatfilm an den Korngrenzen beobachtet werden. Die Anwendbarkeit von durch die Grenzflächenreaktion kontrollierten Lösungs-Kriechmodellen wird diskutiert. Die Abwesenheit stetigen Verformung bei niedrigen Spannungen läßt sich auf die Nicht benetzung des Silikatfilms zurückführen.

Nous avons fabriqué des céramiques de Y-TZP denses et de taille de grains très fine (0.2 μm) par frittage naturel à 1150 °C. Nous avons étudié la déformation superplastique de ces matériaux, en compression, à basse température (1100–1300 °C). Nous avons constaté une augmentation sensible du taux de déformation initial par rapport au matériau disponible dans le commerce, dont la taille de grains est plus grande (0.4 μm, Tosoh, Japan). Un dopage avec de faibles quantités de Fe_2O_3 provoque également une augmentation du taux de déformation. La déformation se produit par un glissement aux joints de grains, contrôlé par la réaction à l'interface. Avant déformation, nous avons pu constater la présence d'un film continu de silicate amorphe aux joints de grains. Nous discutons la pertinence des modèles où le fluage est contrôlé par un processus de solution précipitation à l'interface. Nous attribuons l'absence d'état stationnaire lors de déformations à faibles contraintes au démouillage du film de silicate.

1 Introduction

The potential of fine grained ceramics to exhibit large ductilities at elevated temperatures was already noticed in 1980 from compression tests performed on magnesia.[1] Thereafter, a tensile strain

* To whom correspondence should be addressed.
‡ Present address: Moldinject, Fabrikstrasse 23, CH 3250 Lyss, Switzerland.
§ Present address: Institut de Sciences des Matériaux (I.S.M.A.), Batiment 413–415, Université de Paris sud Centre d'Orsay, F-91405 Orsay Cedex, France.

Journal of the European Ceramic Society 0955-2219/94/$7.00

above 100% was reported for a β-spodumene glass–ceramic material containing some liquid phase.[2] However, the large (170%) tensile strain of 3 mol% Y_2O_3 doped tetragonal zirconia polycrystals (3Y TZP) obtained at 1450°C, as reported by Wakai *et al.*[3] in 1986, is generally regarded as the first convincing evidence for the occurrence of superplasticity in ceramic materials. Since then a considerable amount of research has been performed to investigate the flow characteristics of Y-TZP as a model material; both in tension and in compression. The most important results can be found in recent reviews.[4,5] It has become clear that a very fine grain size (≤ 1 μm) leads to the occurrence of micrograin or structural superplasticity at elevated temperatures in ceramic materials, provided no excessive dynamic grain growth occurs. This is similar to the flow behaviour of superplastic alloys with a grain size smaller than 10 μm.

The large tensile ductilities of this class of ceramic materials offer the exciting possibility to use superplastic forming techniques to fabricate complex shapes with good dimensional control. A variety of superplastic forming techniques[6–9] have now been successfully applied to both single-phase and composite ceramics. To make superplastic forming economically attractive high strain rates at preferably low temperatures are required.

The high temperature deformation behaviour of ceramics is generally characterized in terms of the phenomenological flow law

$$\dot{\varepsilon} = A \exp(-Q/RT) \frac{\sigma^n}{d^p} \qquad (1)$$

where $\dot{\varepsilon}$ is the (axial) strain rate, A a numerical constant, σ the applied stress, n the stress exponent, Q the apparent activation energy, d the grain size, p the grain size exponent and RT has its usual meaning. The mechanisms operating during superplastic flow are identified by determination of the values for the creep parameters n, p and Q together with microstructural observations, such as grain morphology and dislocation substructures.

The research on Y-TZP materials has almost exclusively been focused on commercially available materials (mainly supplied by Tosoh Co. or Daiichi Nippon Kigenso Kagaku Kogyo Co., Japan). These commercial materials can be sintered as received to (nearly) full density at temperatures starting from 1400°C, leading to a minimum grain size of 0.3 μm. Only by hot pressing[6] or elaborate colloidal processing[10] can the sintering temperature be lowered to 1250–1300°C, resulting in a decrease of the grain size to 0·21–0·25 μm.

In this paper it will be shown that, by using an ultrafine powder prepared by a wet chemical method, the sintering can be lowered to 1150°C for Y-TZP. In this way a reduction of the mean grain size to 0.21 μm by normal free sintering has been realized. The reproducibility of the used synthesis method is such that this result can be obtained in a routine like way with all powder batches. It has been investigated whether use of Y-TZP materials fabricated via this route allows a lowering of the superplastic forming temperature (defined as the minimum temperature required for obtaining strain rates $\geq 10^{-4}\,s^{-1}$ under 20 MPa) or alternatively a reduction of forming times due to an increase in strain rates, compared to commercially available materials. Furthermore, it has been examined whether the deformation rates of these materials can be further enhanced by adding a small amount of Fe_2O_3 as a solid solution additive.

The results of compression tests performed on these materials are described here and compared with earlier results obtained by Nauer & Carry[11] on Tosoh materials. The grain boundary chemistry has been found to have a strong impact on the macroscopic deformation behaviour. Grain boundaries of Y-TZP before and after superplastic compression have been intensively studied using X-ray photoelectron spectroscopy (XPS), impedance spectroscopy (IS), scanning Auger microscopy (SAM) and transmission electron microscopy (TEM). The main results of this grain boundary analysis, which are of importance in order to understand the superplastic flow characteristics, are given here. The full analysis will be reported elsewhere.[12]

2 Experimental Procedure

Nanocrystalline (crystallite size 8 nm) zirconia powders doped with 2.6 mol% Y_2O_3 were prepared by a gel precipitation technique, using metal chlorides as precursor chemicals. This so-called chloride method yields very sinter-reactive powders with a low degree of agglomeration. Details of this synthesis method can be found elsewhere.[13] Three 'chloride' powder batches (codenames Chl*x*, where *x* is 1, 2 or 3) were investigated, differing only in residual impurity content (as analysed by flameless AAS). The impurity content of these Chl powder batches and of a 3 mol% yttria-stabilized Tosoh powder (codename TS3/2[14]) is given in Table 1. A part of powder batch Chl3 has been doped with 0.6 mol% $FeO_{1.5}$. A chemisorption technique utilizing iron acetylacetonate ($FeC_{15}H_{21}O_6$) was employed to obtain a homogeneous dispersion of iron. Details of this procedure have been described in Ref. 15.

Green compacts were prepared by cold isostatic compaction in two steps (100 MPa, followed by 400 MPa). Dilatometry (Netzsch 402E dilatometer)

Table 1. Impurity content (wt%) of the powder batches

Powder	Na_2O	Fe_2O_3	Al_2O_3	SiO_2
Ch11	0.004	0.003	0.30	0.062
Ch12	0.006	0.001	0.32	0.236
Ch13	0.010	0.002	0.80	0.010
TS3.2[a]	0.008	0.010	0.005	0.006

[a] Supplier's analysis

was used to compare the densification kinetics of the chloride powders with those supplied by Tosoh. Chloride samples for compression tests all received a final sintering treatment in air at 1150 C for 12–15 h (heating and cooling rate 120 C/h), followed by machining. Specimens of Ch11 and Ch12 were first presintered at 1100 C for 12 h.

Uniaxial compression took place in air at 1100–1300 C under stresses in the range 16–120 MPa. Tests were terminated at true strains of 0.5 to avoid non uniaxial stresses and friction conditions. Axial displacements were measured internally during the tests. Specimen temperatures were monitored by a thermocouple located in the immediate vicinity of the deforming specimens. Sapphire disks were used to avoid direct contact between specimen and SiC pistons. Constant stress experiments were performed on rectangular (7 × 7 × 21 mm) specimens using an Instron testing machine. Specimens were heated at 1000 C/h, followed by heating at 1500 C/h to the desired end temperature. Using such high heating rates prevents microstructural changes from occurring during heating. Additional constant load experiments were performed on cylindrical samples (height 13 mm, diameter 5 mm) using an Elatec hydraulic compression machine. This machine is connected to a Eurotherm FICS 11 controller and a computer equipped with the Eurotherm software package ESP (version 3.22) in a master-slave configuration. A cascade control system (master: load, slave: hydraulic pressure) enables the performance of constant load experiments. The response of the hydraulic system was too slow to perform constant stress experiments. Specimens compressed in the Elatec machine were heated at 1200 C/h to the desired end temperature. At the end of all compression tests the load was quickly removed and samples were cooled down naturally.

Compression of materials Ch11, Ch12 and TS3/2 was performed with the Instron machine, while the pure and iron doped Ch13 material was mainly compressed in the Elatec machine. Comparable results were obtained with both machines during creep tests performed on the Ch13 material, indicating that identical testing conditions could be imposed with both machines. The most important characteristics of samples used for compression tests are given in Table 2.

Table 2. Sintering treatment and characteristics of materials used for compression tests

Material	*Sintering treatment*	*Relative density* (%)	*Grain size* (μm)
Ch11, Ch12	1150 C, 12 h	97	0.21
Ch13, Ch13 + Fe	1150 C, 15 h	96–97	0.15
TS3.2	1450 C, 2 h	99	0.40[10]

The load and displacement readings were converted into true stress and strain rate data. Stress exponents were deduced from strain rates under various stresses using eqn (1) or from individual stress jumps using

$$n = \log\{\dot{\varepsilon}_1/\dot{\varepsilon}_2\}/\{\sigma_1/\sigma_2\}\} \qquad (2)$$

where $\dot{\varepsilon}$ is the strain rate at flow stress σ_1 and $\dot{\varepsilon}_2$ is the strain rate at flow stress σ_2. The values from both techniques were in good agreement with each other. A single specimen was often used for strain rate determinations under several increasing flow stresses.

Densities were measured by the Archimedes technique (in Hg). Grain sizes (d) were determined by the lineal intercept technique from SEM (Hitachi S800) micrographs of polished, thermally etched cuts using $d = 1.56\,L$, where L is the average lineal intercept.

Details of the experimental procedure to characterize grain boundaries of the Ch1 materials using XPS, SAM, IS and TEM are given in Ref. 12.

3 Results

3.1 Undoped Y-TZP

3.1.1 Sintering kinetics

The relative shrinkage during heating at 120 C/h to 1450 C, as measured by dilatometry, of a Ch1 (ρ_{green} = 45%) and a TS3 (ρ_{green} = 52%) compact can be seen in Fig. 1. A significant difference in

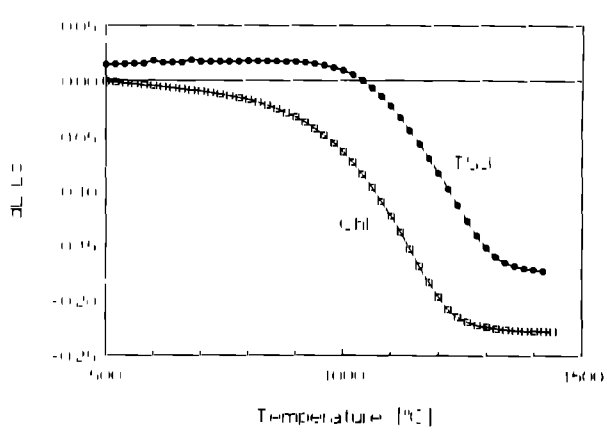

Fig. 1. Relative shrinkage as a function of temperature during heating at 120 C/h of a Ch1 (ρ_{green} = 45%) and TS3 (ρ_{green} = 52%) compact.

sinterability is found: whereas the TS3 sample only starts densifying above 950°C, the Chl specimen densifies already starting from 500°C. The maximum shrinkage rate equals 3×10^{-4} s^{-1} for both specimens (equivalent to a densification rate of 5·4%/min) and is situated at 1150°C and 1230°C for the Chl and the TS3 specimen, respectively. Final densities equal 97–98% for both materials after this sintering schedule. The densification of all three investigated Chl materials was similar.

The Chl specimen reached 96–98% of the theoretical density (6·06 g/cm^3) after isothermal sintering at 1150°C during 10 h (heating rate 120°C/h). By contrast, TS3 samples only reached 73% after the same heat treatment.

3.1.2 *Compression tests*

Strain rates are shown as a function of true strain in Fig. 2 for all three investigated Chl materials during compression at 1250–1300°C under a constant stress of 20 MPa (with stress jumps $20 \rightleftharpoons 16$ MPa and $20 \rightleftharpoons 24$ MPa to determine the stress exponent, the result of which will be mentioned later). The most important observation of Fig. 2 is that no steady state is observed, since the strain rate is decreasing continuously for all three materials. A similar behaviour has been observed at 1100 and 1200°C under constant stresses of 20–40 MPa. During compression at 1200°C under higher stresses (80, 120 MPa) the strain rate remains essentially constant. This apparent work hardening cannot be explained on the basis of grain growth (see Section 3.1.3), but is related to changes in the grain boundary chemistry as will be discussed in Section 4.4.

In the remaining part of this section attention will be focused on the flow behaviour of materials Chl1 and Chl2 and it will be compared to that of the commercial material TS3/2.

Initial strain rates (at strains $\leq 0{\cdot}03$) of Chl1 and Chl2 under 20 MPa are shown in Fig. 3 as a function of inverse temperature. Steady-state strain rates of material TS3/2 are also inserted in this figure. At 1300°C the Chl materials deform initially at strain

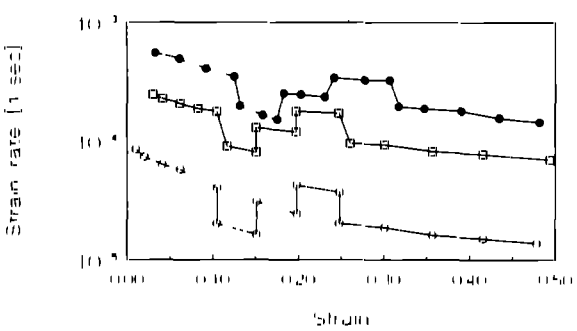

Fig. 2. Strain rates as a function of true strain at 1300°C (□, Chl1; ●, Chl3) and 1250°C (○, Chl2) during compression under a constant stress of 20 MPa (interrupted by stress jumps $20 \rightleftharpoons 16$ and $20 \rightleftharpoons 24$ MPa to determine the stress exponent).

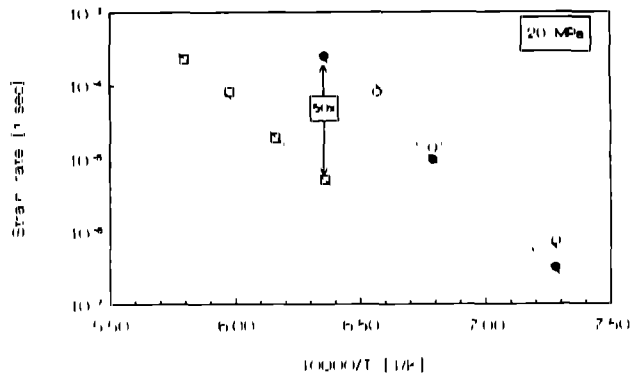

Fig. 3. Temperature dependence of strain rates under 20 MPa of (●) Chl1 and (○) Chl2 (grain size 0·2 μm) and (□) TS3/2 (grain size 0·4 μm). Strain rates of the Chl materials are at strains $\leq 0{\cdot}03$, while those of TS3/2 are steady state values.[10]

rates 50 times faster than observed for the TS3/2 material. The apparent activation energies at 20 MPa as determined from the slope of these curves equal 580 ± 20,[11–14] 596 ± 13 and 540 ± 42 kJ/mol for TS3/2, Chl1 and Chl2, respectively. The temperature dependence of the deformation rate is thus similar for all three materials.

Figure 4 illustrates the variation of strain rate with stress observed during compression under stresses increasing from 20 to 120 MPa at 1200°C of a Chl1 and Chl2 specimen. Slightly higher strain rates are observed for material Chl2, which has a higher impurity content than Chl1 (see Table 1). A stress of 50–60 MPa is required to obtain strain rates larger than 10^{-4} s^{-1} at this temperature. The stress exponent calculated from the slope of these curves equals 2·2–2·3 for both materials. Sudden stress jumps performed at 1100°C ($20 \rightarrow 40$ MPa, not shown) and 1300°C (16–20–24 MPa, see Fig. 2) yield identical values (2·1–2·2) for the stress exponent.

3.1.3 *Microstructural observations*

Examination of the microstructure by SEM after deformation reveals that the grains remain equiaxed at true strains of 0·50 at all investigated temperatures. This observation already shows that grain

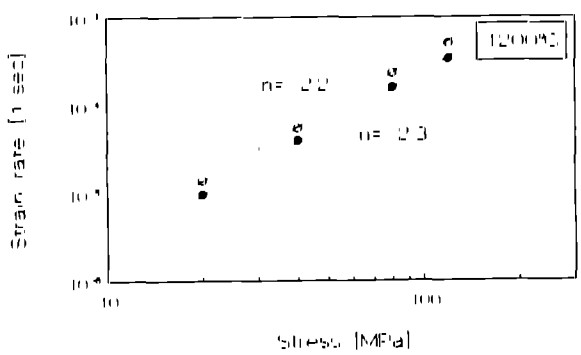

Fig. 4. Stress dependence of the strain rate of a (●) Chl1 and (○) Chl2 specimen at 1200°C during compression under increasing stresses of 20–120 MPa. Strain rates observed immediately after completion of a stress jump have been used here.

boundary sliding is the dominant flow mechanism.[16] Although the final deformation temperature was always situated above the sintering temperature (1150 C), the grain size remained quite stable even at the highest deformation temperature (1300 C). For instance, under 20 MPa at 1300 C (Ch11, 80 min, $\varepsilon = 0.5$) the grain size increased from the initial value of 0.21 μm to 0.26 μm and at 1250 C (Ch12, 350 min, $\varepsilon = 0.5$) it increased to 0.24 μm. No significant difference has been found between samples that were compressed and those which were subjected to the same heat treatment without being compressed.

After the forging treatment all Ch1 samples showed an increase in density to 98–99.5%. Samples which were subjected to the same heat treatment but not compressed, showed no or very little increase in density. Residual porosity can thus be removed by the forming operation itself.

3.1.4 Grain boundary characterization

Grain boundaries in the Ch11 and Ch12 materials before and after compression were characterized by TEM, XPS, SAM and IS. After sintering at 1150 C a thin (9–10 Å) continuous layer of an amorphous phase was observed by TEM along the grain boundaries. XPS and SAM measurements showed that this phase was highly enriched in yttrium. Silicon was detected by XPS and the binding energy indicated that it was present as a silicate. Although powder batch Ch12 contains three times as much silicon as batch Ch11 comparable silicon concentrations were observed at the grain boundaries. Detected silicon concentrations were quite low (Si/Zr ratios less than 0.03). Other main impurities detected were Al^{3+} and F^-. After compressive deformation some grain boundaries were no longer covered by the amorphous phase as observed by TEM. Which fraction of the grain boundaries is 'clean' has not been determined. XPS gave direct proof and IS indirect proof that the average concentrations of impurities and yttrium at the grain boundaries decreased after compressive deformation. This decrease became stronger with increasing stress.

3.2 Compression of Fe_2O_3-doped Y-TZP

Strain rates as a function of applied stress (20–100 MPa), as evaluated from constant load experiments, are shown in Fig. 5 at 1200 and 1300 C for the undoped Ch13 material and at 1200 C for 0.6 mol% $FeO_{1.5}$ doped Ch13. An enhancement in strain rate by a factor of 4–6 compared to the undoped material is observed at 1200 C upon addition of iron. At 20 MPa strain rates of 10^{-4} s^{-1} are observed for this material, while 10^{-3} s^{-1} is reached under 70 MPa.

The stress exponent calculated from the slope of the curves in Fig. 5 equals 1.7–1.8 for undoped Ch13 and 2.2 for the iron doped Ch13 material. The stress exponent calculated from the individual stress jumps at 1200–1300 C (20–100 MPa, Fig. 5 and 16–24 MPa, Fig. 2) of undoped Ch13 equals 2.2–2.3. The stress dependence of the strain rate thus remains unchanged by the addition of iron.

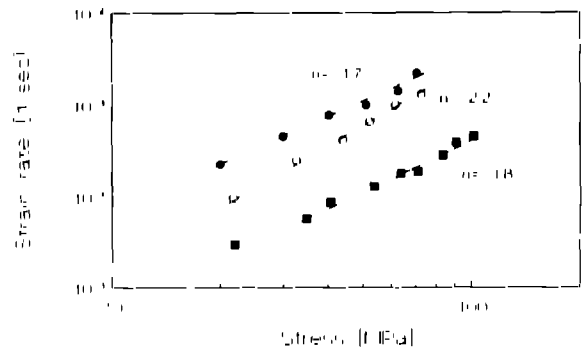

Fig. 5. Stress dependence of the strain rate of the undoped Ch13 material at 1200 C (■) and 1300 C (●) and for $FeO_{1.5}$ dopant level of 0.6 mol% at 1200 C (○) under constant load. Strain rates observed immediately after completion of a stress jump have been used here.

4 Discussion

4.1 Deformation map

Recently, Nauer & Carry[14] proposed a grain size versus stress deformation map for 2Y TZP (batch TS2) at 1350 C. This deformation map is considered valid for Y TZP materials with a relatively high impurity content (> 300 ppm), the deformation behaviour of purer materials being markedly different.[17] Considering the impurity contents of the Ch1 materials (Table 1) the deformation map should also apply for these materials. The exact positions of the boundaries between the various deformation mechanisms however, depend on the nature and amount of residual impurities, as will be discussed later. The deformation map has been recalculated for 1200 C and is shown in Fig. 6. The values of the creep parameters, as given in Ref. 14, are inserted in

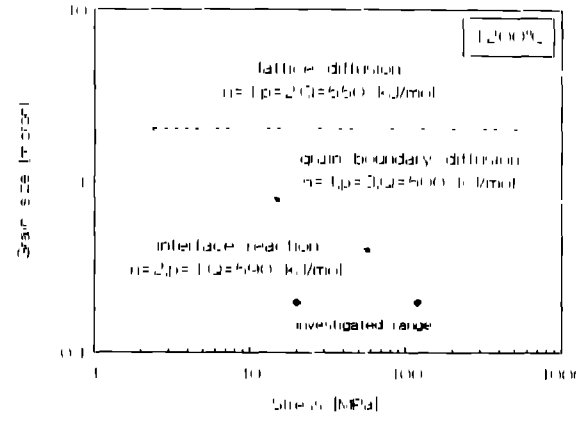

Fig. 6. Deformation map as proposed by Nauer & Carry[14] and recalculated here for 1200 C.

the different fields. It can be seen that the experimental conditions (20–120 MPa at 0·2 μm) of the tests performed with the Chl materials are situated in the interface reaction controlled field. Indeed, the creep parameter values determined here ($n = 2$, $Q = 540$–596 kJ/mol) are in good agreement with the creep parameters of Nauer & Carry for interface reaction control. This suggests that creep of the Chl materials is interface reaction controlled under the investigated experimental conditions. A discussion of the character of the interface reaction will be given in Section 4.3.

The validity of the deformation map is supported by the results of various other researchers. Wakai & Nagano[18] observed a transition from diffusion control to interface reaction control at 1450°C and stresses below 50 MPa, when the grain size was lowered from 1·4 to 0·55 μm. Hwang & Chen[10] performed compression tests at 1100–1250°C in the stress range 50–800 MPa on a 2Y-TZP material with a grain size equal to 0·21 μm. At 1175°C they determined the stress exponent to be equal to 1·6 in the stress range 150–700 MPa and the grain size exponent ($\sigma = 100$ MPa) was 2·7. This clearly indicates grain boundary diffusion control, although part of their stress range is situated in the interface reaction field in the deformation map shown in Fig. 6. Amana *et al.*[19] observed a transition from interface reaction to grain boundary diffusion control above 10 MPa at 1300°C in a 3Y-TZP material ($d = 0{\cdot}60$ μm). This value of the transition stress is slightly lower than the one predicted by the deformation map. It is furthermore worth mentioning that a transition from grain boundary diffusion to lattice diffusion control has recently been observed[20] for 12Ce-TZP at 1250°C if the grain size becomes larger than 2 μm, in good agreement with the deformation map.

Interface reaction controlled and grain boundary diffusion controlled grain boundary sliding are acting in series and the observed strain rate $\dot{\varepsilon}$ can be written as:[21]

$$1/\dot{\varepsilon} = 1/\dot{\varepsilon}_{ir} + 1/\dot{\varepsilon}_{gbd} \qquad (3)$$

where $\dot{\varepsilon}_{ir}$ and $\dot{\varepsilon}_{gbd}$ are the strain rate for respectively the interface reaction controlled and the grain boundary diffusion controlled mechanism. The slowest process determines the deformation rate. It has been shown from experiments that strain rates of Y-TZP are much more sensitive to the impurity content in the interface reaction controlled than in the grain boundary diffusion controlled field[17] (the reasons for this phenomenon are not yet clear). Higher strain rates are observed for more impure materials. The transition from interface reaction to grain boundary diffusion control is therefore influenced by the residual impurity content and this transition will occur at lower stresses for more impure materials. The nature and amount of impurities will thus not influence the general form of the deformation map of 'impure' Y-TZP proposed by Nauer & Carry, but will influence the exact positions of the boundaries between the different fields.

4.2 Strain rate enhancement of Chl in comparison with TS3 materials

The grain size exponent p equals 1 for the TS3/2 material in the interface reaction control field[14,17]. If the strain rates of the Tosoh material are recalculated (using eqn (1) with $p = 1$) for the same grain size (0·2 μm) as the Chl material, an increase in initial strain rate by a factor 25 is still found for the chloride (Chl1, Chl2) materials compared to the TS3/2 material. It should be noted that strain rates of a second Tosoh material (TS3/1[11]) with a higher Al_2O_3 impurity content were faster by a factor of 5 compared to the TS3/2 material for an identical grain size. Clearly, the grain size is not the only factor responsible for the observed differences in strain rates. This difference can arise from the different amounts of impurities in the starting powders (see Table 1) as well as from the difference in sintering temperature of the investigated materials. It is believed that in materials sintered at 1150°C (as is the case for the Chl materials) the segregation of impurities to the grain boundaries is much stronger than in materials sintered at higher temperatures (1400–1450°C, as is the case for the Tosoh materials). Evidence for this hypothesis can be found in the work of Badwal & Hughes,[22] who used XPS and IS to characterize the grain boundary network in cubic ZrO_2–Y_2O_3 and observed that an impurity silicate phase, wetting the grain boundaries at low temperatures, starts to dewet and migrate to the external surface between 1350 and 1450°C. Furthermore, Chen *et al.*[23] found by IS that the grain boundary resistivity per unit surface area of the grain boundaries (R_{sp}) of the Chl materials heat treated at temperatures above 1150°C decreases continuously with temperature, indicating a decrease of the impurity concentrations at the grain boundaries.

4.3 Character of the interface reaction, pressure–solution creep

It has been shown for the Chl materials as well as for the TS3/2 material[14] that deformation is interface reaction controlled in the low stress regime (the width of which depending on grain size, temperature and impurity content), characterized by a stress exponent equal to 2. The grain size exponent equals 1 in this regime[11,17]. A similar σ^2/d dependence of the strain rate has also been observed by Cannon *et al.*[24] for alumina. The character of the interface

reaction and the role of the glassy intergranular film during creep will now be discussed in greater detail

An amorphous phase is present at the grain boundaries as a continuous film having a thickness less than 1 nm or 1.5–2 nm in the Ch1 and the TS3[25] materials, respectively. This film is presumably liquid-like at the temperature of deformation and is able to support moderate normal stresses.[26] It has been reported in the literature that the addition of up to 5 wt% of silicate glasses[27,28] or different amounts of Al_2O_3 or SiO_2 (up to 2.5 wt% of each)[29] enhanced the strain rates, but did not change the stress exponent, which remained equal to 2. In the cited investigations an amorphous phase was present as a thin 1–2 nm film at the grain boundaries and the excess amorphous phase was located at triple points. In the present authors' experiments with the Ch13 material it has also been observed that addition of Fe_2O_3 enhanced the strain rate without changing the stress exponent. The effect of Fe_2O_3 additions on sintering and creep of Y TZP is discussed in more detail elsewhere.[15]

The liquid like film present in virtually all TZPs might allow creep to occur via a solution-precipitation mechanism. Permanent strain would be provided by switching of neighbouring grains during grain boundary sliding, while local strains during the switching event are accomodated by a dissolution–diffusion–precipitation process at the grain boundaries. Theoretical models for solution-precipitation creep (also referred to as 'pressure solution creep' in earth science literature) have been developed by several authors.[30–33] Diffusion through the liquid phase or dissolution-growth of the crystal, i.e. interface reactions, can be rate limiting. To develop models for the interface reaction controlled case, it has been assumed that dissolution or growth of a crystal in an under-supersaturated solution is analogous to the interface reactions occurring during solution-precipitation creep.[34] To the best of the authors' knowledge all models developed so far have assumed that growth or dissolution is linearly proportional to the driving force. During solution-precipitation creep this driving force comes, in a first approximation, from the gradient in the normal tractions along an interface. The gradient equals $2\sigma\Omega/d$,[34] where Ω is the molecular volume and the other symbols have their previously defined meaning. Models assuming linear crystal growth as the interface reaction therefore all lead to a stress exponent equal to 1 for the interface reaction controlled case.

However, available crystal growth theories show that crystal growth rates are only linearly proportional to the driving force if the crystal face is growing above the so-called roughening temperature or if a spiral growth mechanism is operating on a flat face at high values of supersaturation.[35] At small values of supersaturation the crystal growth rate is proportional to the square of the driving force for spiral growth as derived by Burton, Cabrera & Frank (cited in Ref. 35). If this crystal growth mechanism would be rate limiting during solution-precipitation creep, incorporation of the valid crystal growth law into the existing theories for solution-precipitation creep leads to a σ^2/d dependence of the strain rate. This is indeed the dependence observed for Y TZP in the interface reaction control field.

For a spiral growth mechanism the growth rate is directly proportional to the saturation concentration of the liquid[36] (at a constant value of the driving force). If precipitation via spiral growth is rate limiting during solution-precipitation creep, strain rates will scale with the solubility of the solid in the liquid. The composition of the amorphous phase in Y TZP will determine the solubility of zirconia in it and higher solubilities should then lead to higher strain rates. It has indeed been observed recently[28] for Y TZP doped with two types of silicate glasses that the strain rate in the interface reaction control field is proportional to the solubility of zirconia into these silicate glasses.

The macroscopic flow behaviour of Y TZP in the interface reaction control field thus seems to fit well with precipitation controlled solution-precipitation creep with spiral growth as the crystal growth mechanism. However, in the case of superplastic Y TZP, the liquid film has a thickness of only a few nanometers and a spiral growth mechanism is therefore most unlikely because of geometrical reasons. TEM observations have indeed never revealed such spiral structures to exist at the grain boundaries. It is also questionable if the available crystal growth theories formulated for solution growth can be directly applied to precipitation of growth units out of a liquid film of only several nanometers at grain boundaries under deviatory tensile stresses. If crystal growth rates in such a constrained liquid film would be proportional to the square of the driving force without requiring a spiral structure, this would lead to a model for interface reaction controlled solution-precipitation creep in good agreement, both microscopically and macroscopically, with superplastic creep of fine grained Y TZP in the low stress regime. However, such a crystal growth mechanism still has to be established. Most experimental studies of solution-precipitation creep have been performed on materials like NaCl,[33,34] KCl and sucrose,[37] which have a high solubility in the liquid phase (water). The observed stress exponents are equal to 1 in these cases and diffusion through the liquid phase is

considered to be rate limiting during creep of these materials.[33] Creep studies of ceramics with an intentionally 'added' intergranular liquid phase[10,27,29,38] show that interface reactions are rate limiting and observed stress exponents are near 2. The solubility of the studied ceramics in the various liquid phases (silicate melts, containing various cations) has in general not been investigated, but must be quite low, considering the chemical inertness of most technical ceramics. The solubility of the solid in the liquid phase thus seems to be a key parameter during solution–precipitation creep.

The structure of the fluid containing grain boundary of materials with a high solubility in the liquid phase is very much different from the one observed in ceramics. A dynamically stable, island–channel network with a thickness of 500 nm is for instance observed at the grain boundaries of NaCl (grain size 100–275 μm)[39] deformed in the presence of water, while the liquid phase in ceramics is present as a very thin film of a few nanometers.

Future theoretical modelling of creep of ceramics with an intergranular liquid phase should also pay attention to the fact that the physical properties (viscosity, diffusivity) of a liquid in the form of a 1–2 nm film will certainly deviate from its bulk values.

4.4 Dewetting of glassy phase during compressive deformation

The apparent work hardening observed for Chl materials (see Fig. 2) cannot be explained by grain growth (see Section 3.1.3) and is attributed to progressive dewetting of the grain boundary silicate film during compressive deformation. Clarke[26] has formulated a force balance for a thin intergranular liquid film. Without applying an external pressure, the equilibrium thickness is determined by the balance between attractive van der Waals forces and a repulsive force, finding its origin in a epitaxial orientation of the SiO_4 tetrahedra with the grain surfaces. Inserting the appropriate numerical values for the different parameters in Clarke's force balance shows that a compressive stress of 40 MPa is required to remove a liquid silicate film at elevated temperatures from ZrO_2–liquid–ZrO_2 grain boundaries. Considering the large number of simplications in Clarke's theory, this value is in good agreement with the minimum stress of 20 MPa, where dewetting was observed in this investigation.

5 Conclusions

(a) Using nanocrystalline powders produced by the chloride method allows fabrication of dense Y-TZP ceramics with an average grain size of 0·20 μm by free sintering at 1150°C (10 h).

(b) Initial strain rates of these Chl materials during compressive deformation are enhanced by a factor of 50 compared to a coarser-grained (0·40 μm) commercially available (Tosoh Co., Japan) Y-TZP material. This enhancement factor decreases with increasing impurity content of the commercial material.

(c) Under the investigated experimental conditions (1100–1300°C, 16–20 MPa) deformation of these Chl materials occurs via interface reaction controlled grain boundary sliding, in good agreement with the deformation map proposed by Nauer & Carry.

(d) The observed σ^2/d dependence of the strain rate in the interface reaction control field can be predicted from solution-precipitation creep models, if the rate limiting step is precipitation occurring via a mechanism for which the growth rate depends on the square of the driving force. However, available crystal growth theories developed for growth from a bulk mother phase do not provide a non linear mechanism which seems likely for precipitation from a liquid contained in a 1–2 nm thick intergranular film.

(e) Addition of 0·6 mol% $FeO_{1.5}$ leads to a further enhancement of the strain rates of Y-TZP by a factor of 4–6, while the stress exponent remains identical to 2. At 1200°C strain rates of 10^{-3} s^{-1} are obtained at σ = 70 MPa with this material.

Acknowledgements

Akzo Chemicals B.V. is acknowledged for financial support of this investigation. Frank Hartgers and René Olde Scholtenhuis are acknowledged for performing the creep tests on the Chl3 material, Joop Snoeyenbos for machining and polishing, Hans Weber for impurity analysis and Marc Smithers for SEM observations.

References

1 Crampon, J. & Escaig, B., Mechanical properties of fine grained magnesium oxide at large compressive strains. *J. Am. Ceram. Soc.*, **63**(11–12) (1980) 680–6.

2 Wang, J. & Raj, R., Mechanism of superplastic flow in a fine grained ceramic containing some liquid phase. *J. Am. Ceram. Soc.*, **67**(6) (1984) 399–409.

3 Wakai, F., Sakaguchi, S. & Matsuno, Y., Superplasticity of yttria stabilized tetragonal ZrO_2 polycrystal. *Adv. Ceram. Mat.*, **1**(3) (1986) 259–63.

4 Chen, I. W. & Xue, L. A., Development of superplastic structural ceramics. *J. Am. Ceram. Soc.*, **73**(9) (1990) 2585–609.

5 Carry, C., Microstructures, grain boundaries and superplasticity in fine grained ceramics. In *Superplasticity in Metals Ceramics and Intermetallics*, Mat. Res. Soc. Proc. 196, ed. M. Mayo, J. Wadsworth, A. K. Mukherjee & M. Kobayashi. Materials Research Society, Pittsburgh, PA, 1990, pp. 313–23.

6 Carry, C. & Mocellin, A., Examples of superplastic forming of fine grained Al_2O_3 and ZrO_2 ceramics. In *High Tech Ceramics*, ed. P. Vincenzini. Elsevier Science Publishers, Amsterdam, 1987, pp. 1043–62.

7 Kellet, B., High temperature extrusion behavior of fine grain ZrO_2. *J. Mater. Res.*, **5**(10) (1990) 2168–71.

8 Wu, X. & Chen, I. W., Superplastic bulging of fine grained zirconia. *J. Am. Ceram. Soc.*, **73**(3) (1990) 746–9.

9 Wittenauer, J., Nieh, T. G. & Wadsworth, J., A first report on superplastic gas pressure forming of ceramic sheet. *Scr. Met. Mater.*, **26** (1992) 551–6.

10 Hwang, C. & Chen, I. W., Effect of a liquid phase on superplasticity of 2 mol% Y_2O_3 stabilized tetragonal zirconia polycrystal. *J. Am. Ceram. Soc.*, **73**(6) (1990) 1626–32.

11 Nauer, M. & Carry, C., Flow behaviours at high temperature of yttria doped zirconia polycrystals. In *Euro Ceramics*, ed. G. de With, R. A. Terpstra & R. Metselaar. Elsevier Applied Science, London, 1989, pp. 3323–8.

12 Boutz, M. M. R., Winnubst, A. J. A. & Burggraaf, A. J., Characterisation of grain boundaries in superplastically deformed Y TZP ceramics. Submitted to *J. Am. Ceram. Soc.*

13 Groot Zevert, W. F. M., Winnubst, A. J. A., Theunissen, G. S. A. M. & Burggraaf, A. J., *J. Mater. Sci.*, **25** (1990) 3449–55.

14 Nauer, M. & Carry, C., Creep parameters of yttria doped zirconia materials and superplastic deformation mechanisms. *Scr. Met. Mater.* **24** (1990) 1459–63.

15 Boutz, M. M. R., Hartgers, F., Winnubst, A. J. A. & Burggraaf, A. J., Effect of additives on densification and deformation of tetragonal zirconia. Submitted to *J. Mater. Sci.*

16 Ashby, M. F. & Verrall, R. A., Diffusion accommodated flow and superplasticity. *Acta Met.* **21** (1973) 149–63.

17 Nauer, M., Microstructure et superplasticité de zircones yttriées. PhD Thesis No. 996, Ecole Polytechnique de Lausanne, Lausanne, Switzerland, 1992.

18 Wakai, F. & Nagano, T., The role of interface controlled diffusion creep on superplasticity of yttria stabilized ZrO_2 polycrystals. *J. Mater. Sci. Lett.* **7** (1988) 607–9.

19 Amana, B., Duclos, R. & Crampon, J., Stress influence on the deformation mechanisms of tetragonal zirconia polycrystals. *Ceram. Int.* **18** (1992) 385–90.

20 von Minden, C. & Hubner, H., Creep of tetragonal zirconia polycrystals reinforced by alumina platelets. *Euro Ceramics II*, Vol. 2, ed. G. Ziegler & H. Hausner. Deutsche Keramische Gesellschaft e.V., Koln, 1991, pp. 1883–7.

21 Arzt, E., Ashby, M. F. & Verrall, R. A., Interface controlled diffusional creep. *Acta Met.* **31**(12) (1983) 1977–89.

22 Badwal, S. P. S. & Hughes, A. E., The effects of sintering atmosphere on impurity phase formation and grain boundary resistivity in Y_2O_3 fully stabilized ZrO_2. *J. Eur. Ceram. Soc.* **9** (1992) 115–22.

23 Chen, C. S., Boutz, M. M. R., Boukamp, B. A., Winnubst, A. J. A. & Burggraaf, A. J., The electrical characterization of grain boundaries in ultra fine grained Y TZP. *Mater. Sci. Eng. A*, **168** (1993) 231–4.

24 Cannon, R. M., Rhodes, W. H. & Heuer, A. H., Plastic deformation of fine grained alumina I. Interface controlled diffusional creep. *J. Am. Ceram. Soc.*, **63**(1–2) (1980) 46–53.

25 Stoto, T., Nauer, M. & Carry, C., Influence of residual impurities on phase partitioning and grain growth processes of Y TZP materials. *J. Am. Ceram. Soc.*, **74**(10) (1991) 2615–21.

26 Clarke, D. R., On the equilibrium thickness of intergranular glass phases in ceramic materials. *J. Am. Ceram. Soc.*, **70**(1) (1987) 15–22.

27 Yoshizawa, Y. & Sakuma, T., Role of grain boundary glass phase on the superplastic deformation of tetragonal zirconia polycrystal. *J. Am. Ceram. Soc.*, **73**(10) (1990) 3069–73.

28 Gust, M., Goo, G., Wolfenstine, J. & Mecartney, M. L., Influence of amorphous grain boundary phase on the superplastic behavior of 3 mol% yttria stabilized tetragonal zirconia polycrystal (3Y TZP). *J. Eur. Ceram. Soc.*, **76**(7) (1993) 1681–90.

29 Hermansson, T., Swan, H. & Dunlop, G., The role of the intergranular glassy phase in the superplastic deformation of Y TZP Zirconia. In *Euro Ceramics*, ed. G. de With, R. A. Terpstra & R. Metselaar. Elsevier Applied Science, London, 1989, pp. 329–33.

30 Rutter, E. H., The kinetics of rock deformation by pressure solution. *Phil. Trans. Royal Soc. London Series A* **283** (1976) 203–19.

31 Raj, R. & Chung, C. K., Solution precipitation creep in glass ceramics. *Acta Met.* **29** (1981) 159–66.

32 Lehner, F. K. & Bataille, J., Non equilibrium thermodynamics of pressure solution. *Pure Appl. Geophys.*, **122** (1985) 53–85.

33 Spiers, C. J. & Schutjens, P. M. T. M., Densification of crystalline aggregates by fluid phase diffusional creep. In *Deformation Processes in Minerals, Ceramics and Rocks*, ed. D. J. Barber & P. G. Meredith. Unwin Hyman, 1990, pp. 334–53.

34 Raj, R., Creep in polycrystalline aggregates by matter transport through a liquid phase. *J. Geophys. Res.*, **87**(B6) (1982) 4731–9.

35 Bennema, P., Spiral growth and surface roughening: developments since Burton, Cabrera and Frank. *J. Cryst. Growth*, **69** (1984) 182–97.

36 Nielsen, A. E., Electrolyte crystal growth mechanisms. *J. Cryst. Growth*, **67** (1984) 289–310.

37 Pharr, G. M. & Ashby, M. F., On creep enhanced by a liquid phase. *Acta Met.*, **31** (1983) 129–38.

38 Xue, L. A., Effect of liquid forming additives on low temperature superplastic deformation of alumina. *J. Mater. Sci. Lett.* **11** (1992) 1395–7.

39 Spiers, C. J. *et al.*, Experimental determination of constitutive parameters governing creep of rocksalt by pressure solution. In *Deformation Mechanisms, Rheology and Tectonics*, ed. R. J. Knipe & E. H. Rutter. Special Publication No. 54, Geological Society, London, 1990, pp. 215–27.